INTERNAL REPORT

Design, Fabrication and Characterization of a Band-Pass Filter for the S-band of the Sardinia Radio Telescope

Simone Dessì, Giuseppe Valente, Alessandro Fanti,
Enrico Urru, Mauro Pili.

Report N. ,
released: 13 Marzo 2015

Reviewer: Tonino Pisanu

OAC Osservatorio Astronomico di Cagliari

Sommario

1.0 Introduction

Most communication systems contains an RF front end which performs signal processing with RF filters. Microstrip filters are a low cost means of doing this. There is an increasing demand for microwave and millimeter-wave systems to meet the emerging telecommunication challenges with respect to size, performance and cost. Conventional microstrip low pass filters, such as LC-ladder type filter using stepped-impedance transmission line or open-circuited stubs, have been widely used in microwave systems. To obtain an even sharper rate of cutoff for a given number of reactive elements, filters with elliptic function response are often desired, which can give infinite attenuation poles at finite frequency. One way to obtain them is to make use of stepped-impedance lines shunted to the main transmission line to approximate the L-C elements shunted along a transmission line. Microstrip line is a good candidate for filter design due to its advantages of low cost, compact size, light weight and easy integration with other components on a single board.. Because of the increase of radio services, filters are currently widely used in radio astronomy; they allow to protect the allocated bands (by introducing different methods of mitigation and cancellation of interference) and to eliminate the signals in the edges of the bands in order to avoid unwanted intermodulation phenomena that can alter the spectral information of interest in radio astronomy. In this respect, the idea is to insert it, immediately before the first stage of amplification of a radio frequency signal. Tipically such filters can be made with planar devices, usually microstrip lines and with HTS materials that are superconducting already at the criogenic temperatures (<90 K). Exploiting these properties of the material for radioastronomical applications [1], the HTS technology becomes convenient in that the front end of a receiver for radio astronomy is typically cooled to temperatures well below 77 K. This technology also allows to create planar filtering devices with compact dimensions and could provide higher performance not obtainable with any other technology. Obviously, in this case we use high quality substrates, such as the Rogers RO4350E [2], used in this project during the design of the band pass filter. It represents a good candidate for future developments in that it presents very small losses (due to a low dielectric constant) and a good ease of production with a milling machine like the LPKF. In our specific situation, the fabricated filter for image rejection will be inserted into the following receiver chain [3]:

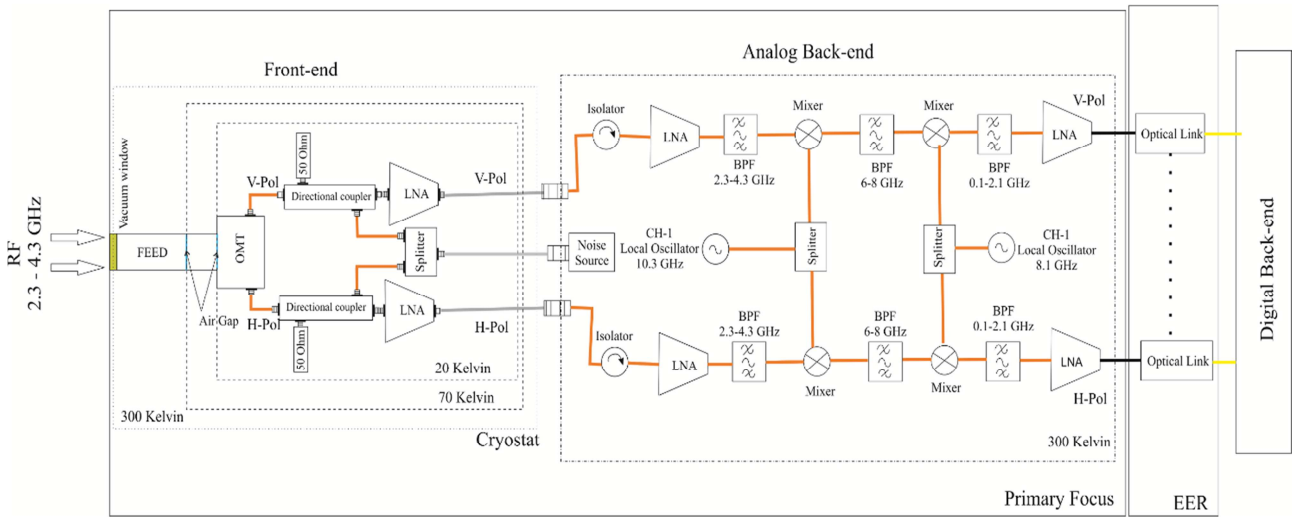

Figure 1. Basic scheme of the S-Band receiver chain in Sardinia Radio Telescope.

A receiver with a poor level of image rejection will suffer from much higher levels of interference than one with a high level of image rejection. In view of this, receivers to be used in high performance applications need to have a good image rejection performance. A receiver with a poor level of image rejection signals means that unwanted signals are received along with the wanted ones and that the levels of interference will be higher than those with a high level of image rejection.

The specifications for the filter under consideration are:

- Bandwidth: 2.3 - 4.3 GHz
- Good attenuation at 4.4 GHz
- Return Loss < -15 dB
- High Compactness
- Rogers RO4350E substrate: ε_r=3.66, h=0.508 mm, tanδ=0.0037, Cu thickness: 0.017 mm

2.0 Theories of filters

2.1 Low pass prototype filters and elements

Filter syntheses for realizing the transfer functions usually result in the so-called low pass prototype filters. A low pass prototype filter is in general defined as the low pass filter whose element values are normalized to make the source resistance or conductance equal to one, denoted by $g_0 = 1$, and the cutoff angular frequency to be unity, denoted by $\omega_c = 1$(rad/s). For example, Fig. 2 demonstrates two possible forms of an *n*-pole low pass prototype for realizing an all-pole filter response, including Butterworth, Chebyshev, and Gaussian responses. Either form may be used because both are dual from each other and give the same response. It should be noted that in Fig. 2, g_i for $i = 1$ to n represent either the inductance of a series inductor or the capacitance of a shunt capacitor; therefore, n is also the number of reactive elements. If g_1 is the shunt capacitance or the series inductance, then g_0 is defined as the source resistance or the source conductance.

Similarly, if g_n is the shunt capacitance or the series inductance, g_{n+1} becomes the load resistance or the load conductance. This type of low pass filter can serve as a prototype for designing many practical filters with frequency and element transformations.

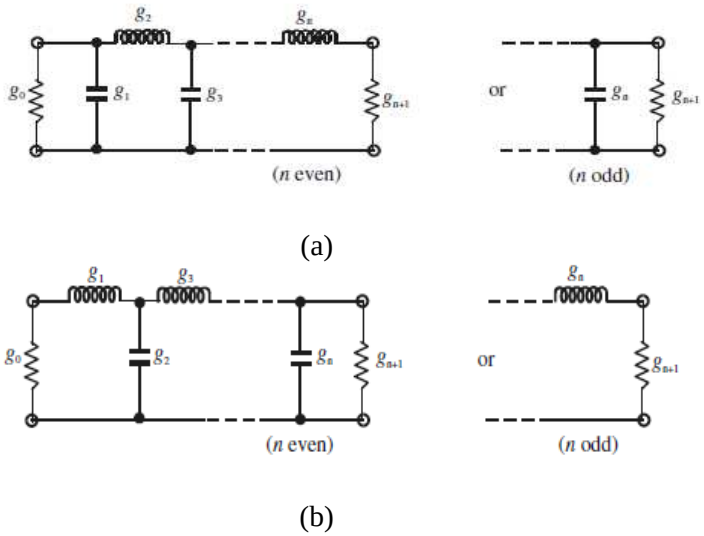

Figure 2. Low pass prototype filters for all-pole filters with (a) a ladder network structure and (b) its dual

2.2 Frequency and element transformations

The frequency transformation, which is also referred to as frequency mapping, is required to map a response such as Chebyshev response in the low pass prototype frequency domain Ω to that in the frequency domain ω in which a practical filter response such as low pass, high pass, band pass, and band stop are expressed. The frequency transformation will have an effect on all the reactive elements accordingly, but no effect on the resistive elements. In addition to the frequency mapping, impedance scaling is also required to accomplish the element transformation. The impedance scaling will remove the $g_0 = 1$ normalization and adjust the filter to work for any value of the source impedance denoted by Z_0. For our formulation, it is convenient to define an impedance scaling factor γ_0 as

$$\gamma_0 = Z_0 / g_0 \quad \text{for } g_0 \text{ being the resistance}$$
$$\gamma_0 = g_0 / Y_0 \quad \text{for } g_0 \text{ being the conductance}$$

where $Y_0 = 1/Z_0$ is the source admittance. In principle, applying the impedance scaling upon a filter network in such a way that

$$L \rightarrow \gamma_0 L$$
$$C \rightarrow C/\gamma_0$$
$$R \rightarrow \gamma_0 R$$
$$G \rightarrow G/\gamma_0$$

has no effect on the response shape. Let g be the generic term for the low pass prototype elements in the element transformation to be discussed. Because it is independent of the frequency transformation, the following resistive element transformation holds for any type of filter:

$$R = \gamma_0 g \quad \text{for g representing the resistance}$$
$$G = g/\gamma_0 \quad \text{for g representing the conductance}$$

2.3 Band pass transformation

Assume that a low pass prototype response is to be transformed to a band pass response having a passband $\omega_2 - \omega_1$, where ω_1 and ω_2 indicate the pass band-edge angular frequency. The required frequency transformation is

$$\Omega = \frac{\Omega_c}{FBW}\left(\frac{\omega}{\omega_0} - \frac{\omega_0}{\omega}\right) \tag{1}$$

with

$$\text{FBW} = \frac{\omega_2 - \omega_1}{\omega_0} \qquad \omega_0 = \sqrt{\omega_1 \omega_2} \tag{2}$$

where ω_0 denotes the center angular frequency and *FBW* is defined as the fractional bandwidth. If we apply this frequency transformation to a reactive element g of the low pass prototype, we have

$$j\Omega g \rightarrow j\omega \frac{\Omega_c\, g}{FBW\ \omega_0} + \frac{1}{j\omega}\frac{\Omega_c\, \omega_0\, g}{FBW}$$

which implies that an inductive/capacitive element g in the low pass prototype will transform to a series/parallel LC resonant circuit in the band pass filter. The elements for the series LC resonator in the band pass filter are

$$L_s = \left(\frac{\Omega_c}{FBW\ \omega_0}\right) \gamma_0\, g \quad , \quad C_s = \left(\frac{FBW}{\Omega_c\ \omega_0}\right) \frac{1}{\gamma 0\ g} \qquad \text{for } g \text{ representing the inductance}$$

where the impedance scaling has been taken into account as well. Similarly, the elements for the parallel LC resonator in the band pass filter are

$$L_p = \left(\frac{FBW}{\Omega_c \omega_0}\right) \frac{\gamma 0}{g} \quad , \quad C_p = \left(\frac{\Omega_c}{FBW\ \omega_0}\right) \frac{g}{\gamma 0} \qquad \text{for } g \text{ representing the capacitance}$$

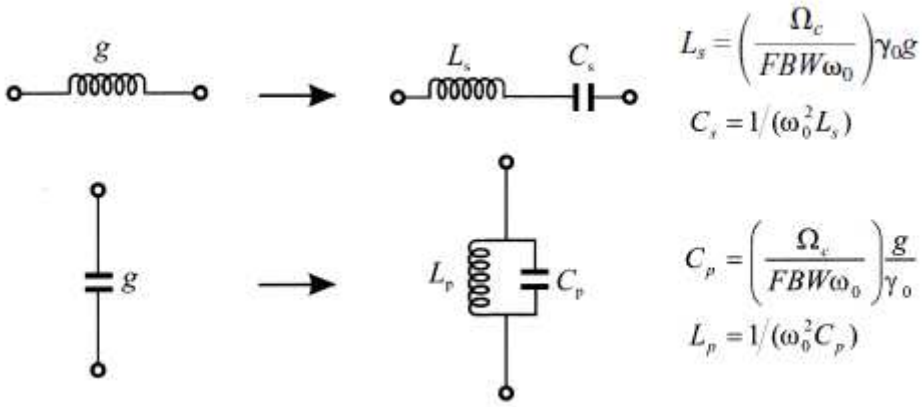

Figure 3. Low pass prototype to band pass transformation: basic element transformation

2.4 Immittance inverters

Immittance inverters are either impedance or admittance inverters. An idealized impedance inverter is a two-port network that has a unique property at all frequencies, i.e., if it is terminated in an impedance Z_2 on one port, the impedance Z_1 seen looking in at the other port is

$$Z_1 = \frac{K^2}{Z_2}$$

where K is real and defined as the characteristic impedance of the inverter. As can be seen, if $Z2$ is inductive/conductive, $Z1$ will become conductive/inductive, and hence the inverter has a phase shift of ±90 degrees or an odd multiple thereof. Impedance inverters are also known as K-inverters. The $ABCD$ matrix of ideal impedance inverters may generally be expressed as

$$\begin{bmatrix} A & B \\ C & D \end{bmatrix} = \begin{bmatrix} 0 & \mp jK \\ \mp \frac{1}{jK} & 0 \end{bmatrix}$$

Likewise, an ideal admittance inverter is a two-port network that exhibits such a property at all frequency that if an admittance Y_2 is connected at one port, the admittance Y_1 seen looking in the other port is

$$Y_1 = \frac{J^2}{Y_2}$$

where J is real and called the characteristic admittance of the inverter. Similarly, the admittance inverter has a phase shift of ±90 degrees or an odd multiple thereof. Admittance inverters are also referred to as *J*-inverters. In general, ideal admittance inverters have the *ABCD* matrix

$$\begin{bmatrix} A & B \\ C & D \end{bmatrix} = \begin{bmatrix} 0 & \pm\frac{1}{jJ} \\ \mp jJ & 0 \end{bmatrix}$$

2.5 Richards' transformation and Kuroda identities

Distributed transmission line elements are of importance for designing practical microwave filters. A commonly used approach to the design of a practical distributed filter is to seek some approximate equivalence between lumped and distributed elements. Such equivalence can be established by applying Richards's transformation. Richards showed that distributed networks, comprised of commensurate length (equal electrical length) transmission lines and lumped resistors, could be treated in analysis or synthesis as lumped element *LCR* networks under the transformation

$$t = \tanh\frac{lp}{v_p} \tag{3}$$

where $p = \sigma + j\omega$ is the usual complex frequency variable, and l/v_p is the ratio of the length of the basic commensurate transmission line element to the phase velocity of the wave in such a line element; t is a new complex frequency variable, also known as Richards' variable. The new complex plane where t is defined is called the t-plane. Equation (3) is referred to as Richards' transformation. For lossless passive networks $p = j\omega$ and the Richards' variable is simply expressed by

$$t = j\tan\Theta$$

where $\Theta = \frac{\omega}{v_p} l$ is the electrical length.

Assuming that the phase velocity v_p is independent of frequency, which is true for TEM transmission lines, the electrical length is then proportional to frequency and may be expressed as $\Theta = \Theta_0\omega/\omega_0$, where Θ_0 is the electrical length at a reference frequency ω_0. It is convenient for discussion to let ω_0 be the radian frequency at which all line lengths are quarter-wave long with $\Theta_0 = \pi/2$ and to let $\Omega = \tan\Theta$, so that

$$\Omega = \tan\left(\frac{\pi}{2}\frac{\omega}{\omega_0}\right)$$

As ω varies between 0 and ω_0, Ω varies between 0 and ∞, and the mapping from ω to Ω is not one to one but periodic, corresponding to the periodic nature of the distributed network.

Under Richards' transformation, a close correspondence exists between lumped inductors and capacitors in the p-plane and short- and open-circuited transmission lines in the t-plane. As a one-port inductive element with an impedance $Z = pL$, a lumped inductor corresponds to a short-circuited line element (stub) with an input impedance $Z = tZc = jZc \tan\Theta$, where Zc is the characteristic impedance of the line. Likewise, a lumped capacitor with an admittance $Y = pC$ corresponds to an open-circuited stub of input admittance $Y = tYc = jYc \tan\Theta$ and characteristic admittance Yc. In designing transmission line filters, various network identities may be desirable to

obtain filter networks that are electrically equivalent, but that differ in form or in element values. Such transformations not only provide designers with flexibility, but also are essential in many cases to obtain networks that are physically realizable with physical dimensions. The Kuroda identities form a basis to achieve such transformations, where the commensurate line elements with the same electrical length Θ are assumed for each identity. The first two Kuroda identities interchange a unit element with a shunt open-circuited stub or a series short-circuited stub, and a unit element with a series short-circuited stub or a shunt open-circuited stub. The other two Kuroda identities, involving the ideal transformers, interchange stubs of the same kind.

3.0 Band pass filters design method

3.1 Parallel coupled, Half wavelength resonators filters

This particular implementative technique is applicable only to band pass filters. The parallel or series resonators, are made with $\lambda_0/2$ line sections and the inverters are made by coupling these lines between them longitudinally. Fig. 4 illustrates a general structure of parallel-coupled (or edge-coupled) microstrip band pass filters that use half-wavelength line resonators. They are positioned so that adjacent resonators are parallel to each other along half of their length. This parallel arrangement gives relatively large coupling for a given spacing between resonators, and thus, this filter structure is particularly convenient for constructing filters having a wider bandwidth as compared to the structure for the end coupled. Regarding the project, the first step is to choose the value of series components and the characteristic impedance of the line; the matching will be in general different for each inverter. The filter is designed diagonally in such a way as to optimize the space occupied on the substrate. However, through different simulations, it has been demonstrated that this particularity is not an essential feature for the purposes of the filter response. To obtain filters with low Q (therefore with a large bandwidth) it is necessary to decrease the coupling space between the lines and this may be limited by technological processes of printing of the conductor. The design equations for this type of filter are given by

$$
\begin{aligned}
Z_0 J_{01} &= \sqrt{\frac{\pi}{2}\frac{\Delta}{g_0 g_1}} \\
Z_0\, J_{12} &= \frac{\pi\Delta}{2\sqrt{g_1 g_2}} \\
Z_0\, J_{23} &= \frac{\pi\Delta}{2\sqrt{g_2 g_3}} \\
&\cdots \\
Z_0\, J_{n,\,n+1} &= \sqrt{\frac{\pi}{2}\frac{\Delta}{g_n g_{n+1}}}
\end{aligned}
\qquad (4)
$$

where g_o, g_1 . . . g_n are the elements of a ladder-type low pass prototype with a normalized cutoff Ω_c=1, and Δ is the fractional bandwidth of the band pass filter; $Jj,j+1$ are the characteristic admittances of *J*-inverters and Z_0 is the characteristic impedance of the terminating lines (50 Ω). To realize the *J*-inverters obtained above, the even- and odd-mode characteristic impedances of the coupled microstrip line resonators are determined by

$$Z_{0\ even\ 0,1} = Z_0\ [1+Z_0 J_{0,1}+(Z_0\ J_{0,1})^2] \quad (5)$$
$$Z_{0\ odd\ 0,1} = Z_0\ [1-Z_0\ J_{0,1}+(Z_0\ J_{0,1})^2]$$
$$Z_{0\ even\ 1,2} = Z_0\ [1+Z_0\ J_{1,2}+(Z_0\ J_{1,2})^2]$$
$$Z_{0\ odd\ 1,2} = Z_0\ [1-Z_0\ J_{1,2}+(Z_0\ J_{1,2})^2]$$
…

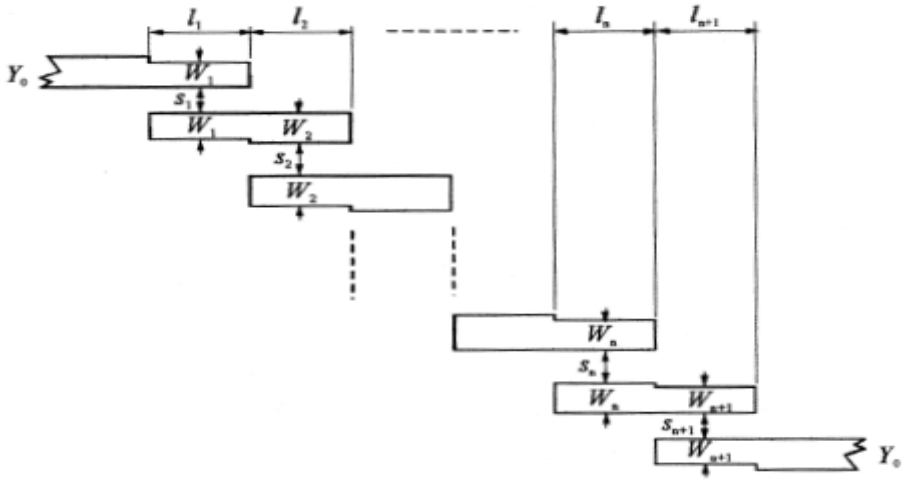

Figure 4. General structure of the band-pass filter with parallel coupled lines.

After an initial study with the software Advanced Design System, a low-pass prototype with Chebyshev response has been chosen, whose element values, for n=7 and pass-band ripple L_{AR}=0.1dB, are:

$g_0=g_8$	$g_1=g_7$	$g_2=g_6$	$g_3=g_5$	g_4
1	1.1812	1.4228	2.0967	1.5734

Table 1. Chebyshev coefficients for n=7 and ripple 0.1 dB.

Using the element transformations, the inductance and capacitance values are listed in Table 2.

$$L_i' = \frac{g_i(50)}{\Delta\omega_0} \quad \text{for series branches} \quad (6)$$
$$C_i' = \frac{\Delta}{50\ \omega_0 g_1}$$

$$L_j' = \frac{\Delta(50)}{g_2\omega_0} \quad \text{for parallel branches}$$
$$C_j' = \frac{g_2}{50\Delta\ \omega_0}$$

where $FBW=\Delta=\frac{\omega 2-\omega 1}{\omega_0}$ = 60 %

$L_1'=L_7'$	$C_1'=C_7'$	$L_2'=L_6'$	$C_2'=C_6'$	$L_3'=L_5'$	$C_3'=C_5'$	L_4'	C_4'
4.749 nH	0.490 pF	1.017 nH	2.288 pF	8.431 nH	0.276 pF	0.920 nH	2.530 pF

Table 2. Inductance and capacitance values.

The constants of the inverters and the characteristic impedances of the even and odd modes are listed in the following tables:

$Z_0 J_{01}$	$Z_0 J_{12}$	$Z_0 J_{23}$	$Z_0 J_{34}$	$Z_0 J_{45}$	$Z_0 J_{56}$	$Z_0 J_{67}$	$Z_0 J_{78}$
0.893	0.726	0.545	0.518	0.518	0.545	0.726	0.893

Table 3. Inverters constants.

$Z_{0\ even\ 0,1}$ = $Z_{0\ even\ 7,8}$	$Z_{0\ odd\ 0,1}$ = $Z_{0\ odd\ 7,8}$	$Z_{0\ even\ 1,2}$ = $Z_{0\ even\ 6,7}$	$Z_{0\ odd\ 1,2}$ = $Z_{0\ odd\ 6,7}$	$Z_{0\ even\ 2,3}$ = $Z_{0\ even\ 5,6}$	$Z_{0\ odd\ 2,3}$ = $Z_{0\ odd\ 5,6}$	$Z_{0\ even\ 3,4}$ = $Z_{0\ even\ 4,5}$	$Z_{0\ odd\ 3,4}$ = $Z_{0\ odd\ 4,5}$
134.52 Ω	45.22 Ω	112.65 Ω	40.05 Ω	92.10 Ω	37.60 Ω	89.31 Ω	37.51 Ω

Table 4. Characteristic impedances of the even and odd modes.

The next step of the filter design is to find the dimensions of the coupled microstrip lines that exhibit the desired even- and odd-mode impedances. For instance, referring to Fig. 4, W_1 and s_1 are determined such that the resultant even- and odd mode impedances match to $(Z_0e)_{0,1}$ and $(Z_0o)_{0,1}$. Assume that the microstrip filter is constructed on a Rogers RO4350E substrate with a relative dielectric constant of 3.66 and thickness of 0.508 mm. The dielectric loss tangent is tanδ=0.0037.

The choice of this type of substrate is essentially due to the low loss (low dielectric constant) and to the ease of manufacturing with the LPKF; furthermore, this type of substrate allows the integration of multiple SMD components on a single board. Using the design equations for coupled microstrip lines given in Chapter 4 [4], the optimized dimensions for each pair of quarter-wavelength coupled sections were found (Table 5).

W_1=W_7	l_1=l_7	S_1=S_7	W_2=W_6	l_2=l_6	S_2=S_6	W_3=W_5	l_3=l_5	S_3=S_5	W_4	l_4	S_4
0.162	14.599	0.059	0.245	14.498	0.0473	0.475	14.262	0.038	0.511	14.228	0.040

Table 5. Optimized dimensions of the Band pass filter with parallel coupled lines.

3.1.1 Simulation and measured results

The design is verified with the Sonnet EM Simulation, a full-wave analysis engine which takes into account all possible coupling mechanisms. The layout of the microstrip filter with the final design dimensions is given in Fig. 5, the simulated frequency response is shown in Fig. 6 while the 3D view of the simulated filter is given in Fig. 7.

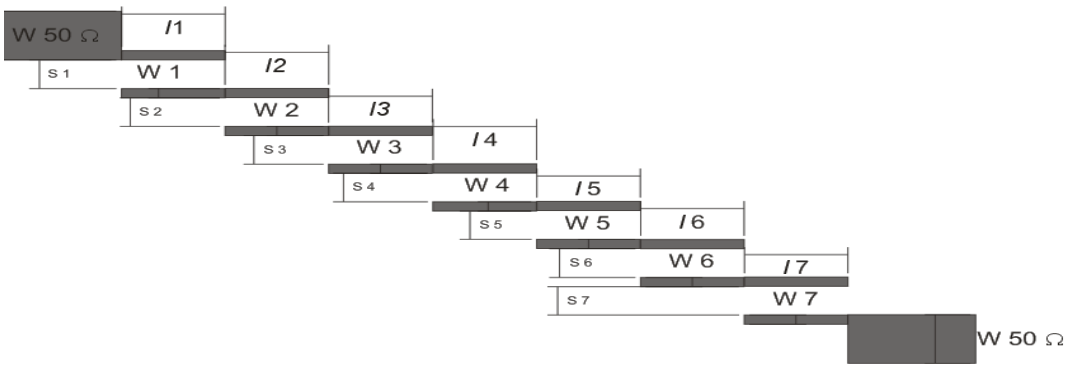

Figure 5. Layout of a 7-pole parallel coupled microstrip band pass filter on a Rogers RO4350E substrate with ε_r = 3.66 and h=0.508 mm.

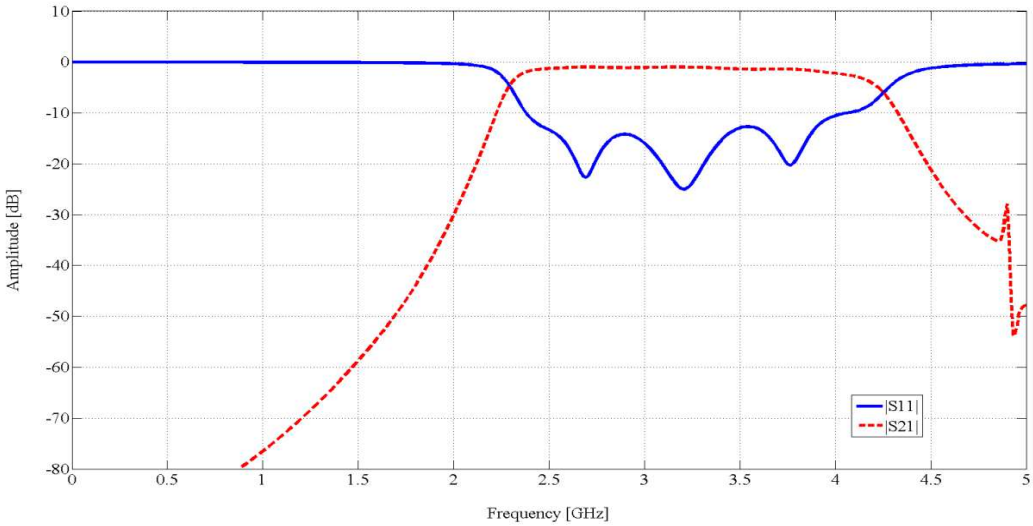

Figure 6. Simulated frequency response of the parallel coupled band pass filter: S_{11} parameter (continuous line), S_{21} parameter (dashed line).

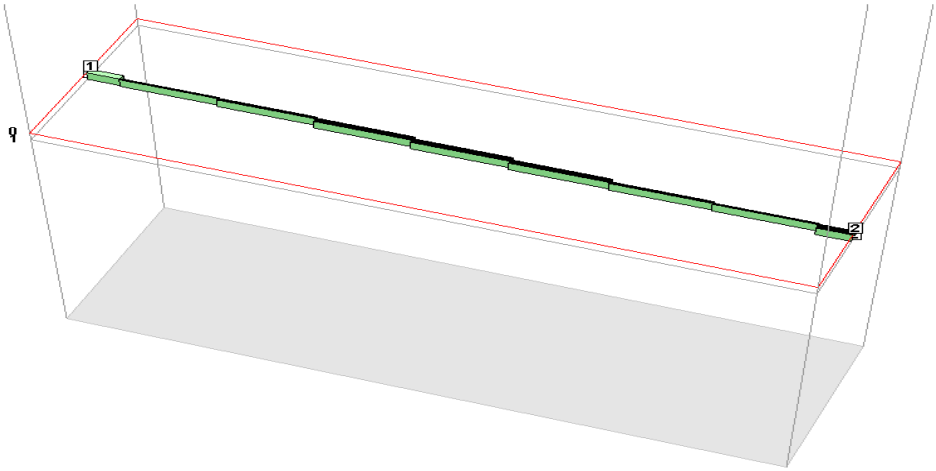

Figure 7. 3D view of the parallel coupled band pass filter.

3.1.2 Considerations

From Fig. 6 it is evident that the bandwidth, although similar to the desired one, and although presenting a slope such as to ensure a good selectivity, shows to be lower than the desired one. In addition, the optimized spacing values are not physically realizable because they are smaller than the threshold permitted by the LPKF ProtoMat C100 HF (0.5 mm). The simulated coupled lines band pass filter, therefore, does not allow to obtain a very wide bandwidth as that required by the specifications. To overcome this problem, it has been decided to study a different configuration.

3.2 Lambda/4 short-circuited stubs filter

We studied a configuration which is comprised of shunt short-circuited stubs that are $\lambda/4$ long with connecting lines that are also $\lambda/4$ long, where λ_0 is the guided wavelength in the medium of propagation at the midband frequency f_0.
A low pass prototype filter with Chebyshev response is chosen, for n = 7 and 0.1 dB ripple, and it has been obtained the transformed band pass circuit with lumped parameters (Fig. 8):

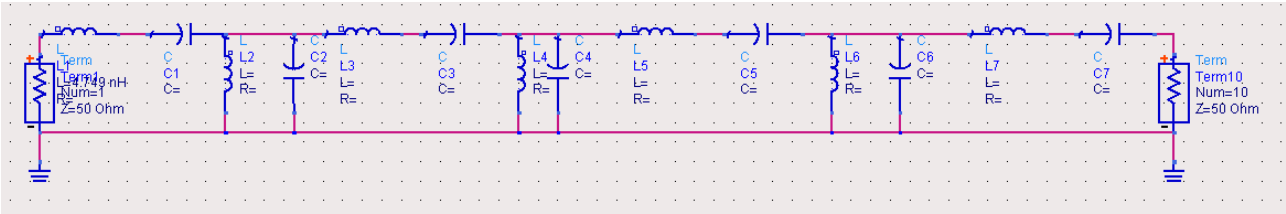

Figure 8. Layout of the band pass filter with lumped parameters.

We chose a design approach that considers a line of constant characteristic impedance in which lines with variable characteristic impedance are applied. The line sections were then optimized with the use of a simulation software tools such as Advanced Design System and Sonnet. The parameters of the low pass prototype are shown in the following table:

$g_0=g_8$	$g_1=g_7$	$g_2=g_6$	$g_3=g_5$	g_4
1	1.1812	1.4228	2.0967	1.5734

Table 6. Chebyshev coefficients for n=7 and ripple 0.1 dB.

Using the element transformations:

$L_i' = \frac{g_i(50)}{\Delta\omega_0}$ for series branches

$C_i' = \frac{\Delta}{50\ \omega_0 g_1}$

$L_j' = \frac{\Delta(50)}{g_2\omega_0}$ for parallel branches

$C_j' = \frac{g_2}{50\Delta\ \omega_0}$

$L_1'=L_7'$	$C_1'=C_7'$	$L_2'=L_6'$	$C_2'=C_6'$	$L_3'=L_5'$	$C_3'=C_5'$	L_4'	C_4'
4.749 nH	0.490 pF	1.017 nH	2.288 pF	8.431 nH	0.276 pF	0.920 nH	2.530 pF

Table 7. Inductance and capacitance values.

The design equations for this type of filter are given by

$$Z_0 J_{01} = \sqrt{\frac{\pi}{4}\frac{\Delta}{g_0 g_1}} \qquad (7)$$

$$Z_0\ J_{12} = \frac{\pi\Delta}{4\sqrt{g_1 g_2}}$$

$$Z_0\ J_{23} = \frac{\pi\Delta}{4\sqrt{g_2 g_3}}$$

$\cdots$

$$Z_0\ J_{n,\,n+1} = \sqrt{\frac{\pi}{4}\frac{\Delta}{g_n g_{n+1}}}$$

where *go*, *g*1 . . . *gn* are the elements of a ladder-type low pass prototype with a normalized cutoff Ω_c=1, and Δ is the fractional bandwidth of the band pass filter; *Jj*,*j*+1 are the characteristic admittances of *J*-inverters and Z_0 is the characteristic impedance of the terminating lines (50 Ω). The inverters constants are listed in table 8.

$Z_0 J_{01}$	$Z_0 J_{12}$	$Z_0 J_{23}$	$Z_0 J_{34}$	$Z_0 J_{45}$	$Z_0 J_{56}$	$Z_0 J_{67}$	$Z_0 J_{78}$
0.631	0.363	0.272	0.259	0.259	0.272	0.363	0.631

Table 8. Inverters constants.

For a pass band filter with short-circuited stubs filter, the characteristic impedances are given by

$$Z_{0n}= \frac{\pi \Delta Z_0}{4 g_n} \qquad n = 1 \text{ e } 2 \qquad (8)$$

This expression is only applicable to filters with input and output impedance equal to Z_0, and it can't be used for projects that provide a constant ripple with even order.

$Z_{0,1}$	$Z_{0,2}$	$Z_{0,3}$	$Z_{0,4}$	$Z_{0,5}$	$Z_{0,6}$	$Z_{0,7}$
19.94 Ω	16.55 Ω	11.23 Ω	14.97 Ω	11.23 Ω	16.55 Ω	19.94 Ω

Table 9. Characteristic impedances for the pass band filter with short-circuited stubs.

The values of the characteristics impedances allow to calculate the widths of the stubs through the design equations presented in Cap.4 [4].

- $Z\sqrt{\varepsilon_r} > 89.91$

$$\frac{W}{h} = \frac{8\exp(A)}{\exp(2A)-2} \qquad \text{where} \qquad A= \frac{Z0}{60}\sqrt{\frac{\varepsilon_r+1}{2}} + \frac{\varepsilon_r-1}{\varepsilon_r+1}\left[0.23 + \frac{0.11}{\varepsilon_r}\right]$$

- $Z\sqrt{\varepsilon_r} < 89.91$

$$\frac{W}{h} = \frac{2}{\pi}\left\{ B - 1 - \ln(2B-1) + \frac{\varepsilon_r - 1}{2\varepsilon_r}\left[\ln(B-1) + 0.39 - \frac{0.61}{\varepsilon_r}\right]\right\}$$

$$B = \frac{60\,\pi^2}{Z\sqrt{\varepsilon_r}}$$

Section l_i [mm]	W_i [mm] [initial]	W_i [mm] [optimized]
$l_1 = 14.00$	3.92	1.2
$l_2 = 13.10$	1.1	1.5
$l_3 = 13.50$	4.91	2
$l_4 = 13.20$	1.1	1.5
$l_5 = 13.90$	7.71	2.2
$l_6 = 13.30$	1.1	1.4
$l_7 = 13.30$	5.53	2.6
$l_8 = 13.20$	1.1	1.4
$l_9 = 13.90$	7.71	2.2
$l_{10} = 13.20$	1.1	1.5
$l_{11} = 13.50$	4.91	2
$l_{12} = 13.10$	1.1	1.5
$l_{13} = 14.00$	3.92	1.2
$l_{50\Omega} = 5$	1.1	1.1

Table 10. Initial and optimized design parameters of microstrip lines.

3.2.1 Simulation and measured results

The design was initially verified, with Advanded Design System software and then, more accurately, with the Sonnet EM Simulation. The layout of the microstrip filter with the final design dimensions is given in Fig. 9, the 3D view of the simulated filter is given in Fig. 10 while the simulated frequency response is shown in Fig. 11.

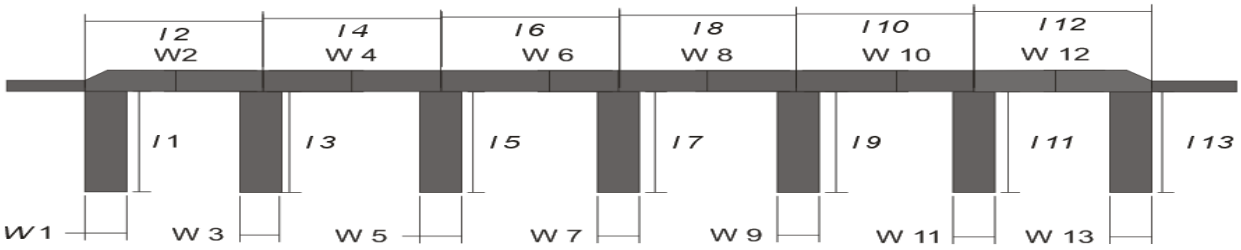

Figure 9. Layout of the simulated band pass filter.

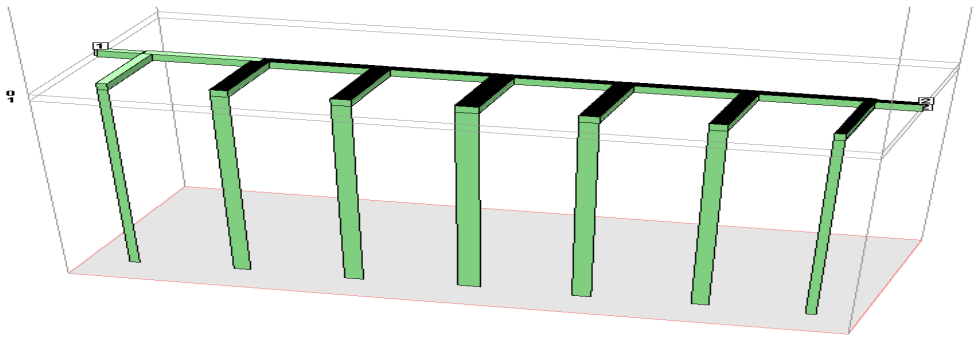

Figure 10. 3D view of the simulated band pass filter..

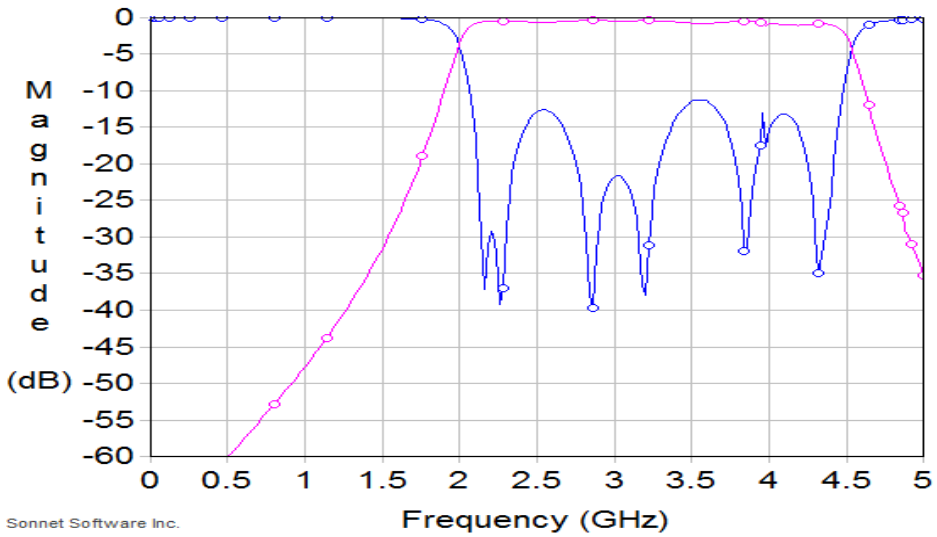

Figure 11. Layout of a 7-pole microstrip band pass filter with short-circuited stubs on a Rogers RO4350E substrate with $\varepsilon_r = 3.66$ and h=0.508 mm.

3.2.2 Considerations

The simulated filter presents a good improvement compared to the configuration with coupled parallel lines. It's evident an high increase of the bandwidth but despite this the frequency response doesn't meet the initial specifications (bandwidth is greater than 2 GHz); for this reason, it has been studied a modified configuration with the addition of three short-circuited stubs, positioned in such a way as to ensure a decrease of the bandwidth and to improve the selectivity.

3.2.3 Modified configuration with additional stubs

The modified layout is shown in Fig. 12.

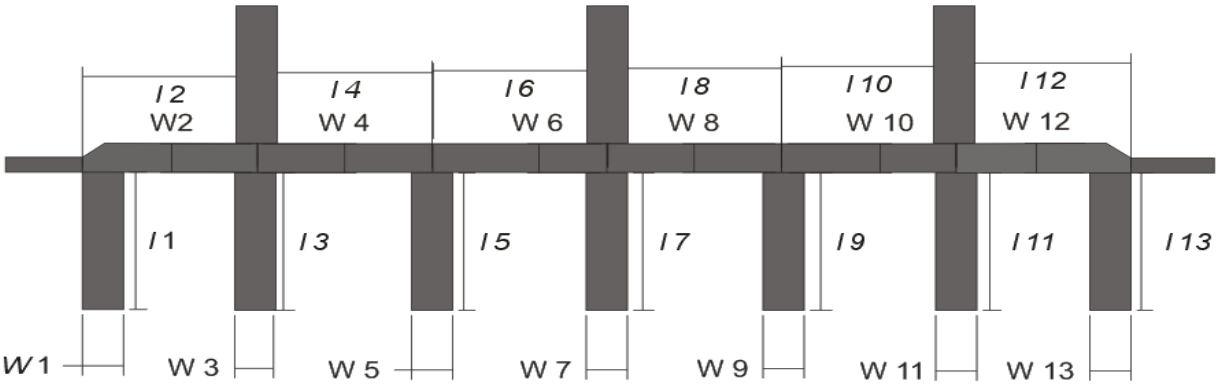

Figure 12. Modified layout of the band pass filter with short-circuited stubs.

This solution allows to decrease the bandwidth (2 GHz, with cutoff frequencies 2.3 GHz and 4.3 GHz). The simulated filter has been fabricated with the LPKF ProtoMat C100 HF; this step needs attention about the choice of the cutting tools (for the accurate definition of the metal stripes). It has been used the SMA connector R125.423.200, whose datasheet is available on Radiall [5]. The

paths to ground were made by welding; in this step we found some difficulties due to the thickness of the substrate (0.508 mm). In addition, paths to ground could be more precise with the use of conductive glue. The fabricated filter has been tested by measurement using a ROHDE&SCHWARZ ZVA 67 Vector Network Analyzer and the ZVZ218 calibration kit.

The comparison between simulated and measured frequency response of this microstrip filter is illustrated in Fig. 13 while the fabricated band pass filter is given in Fig. 14.

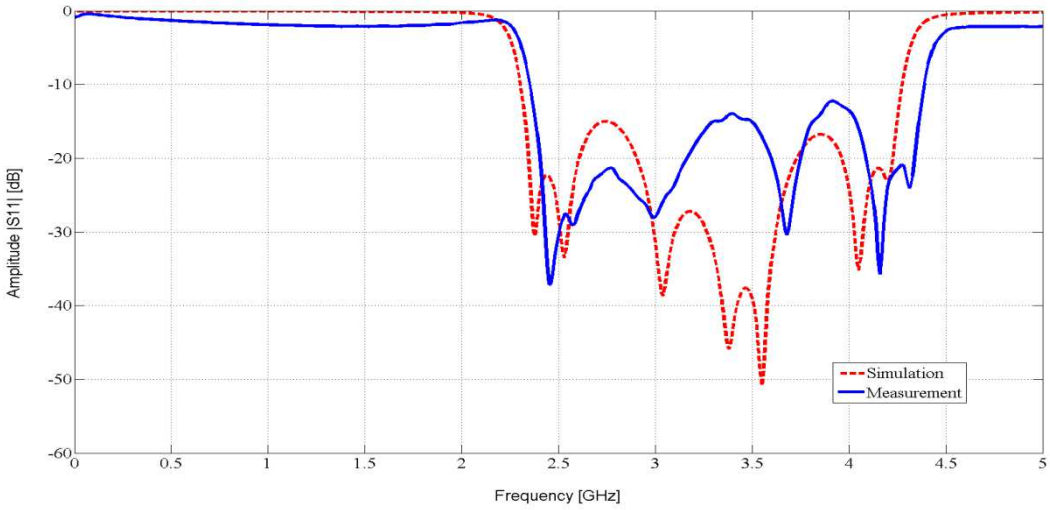

(a)

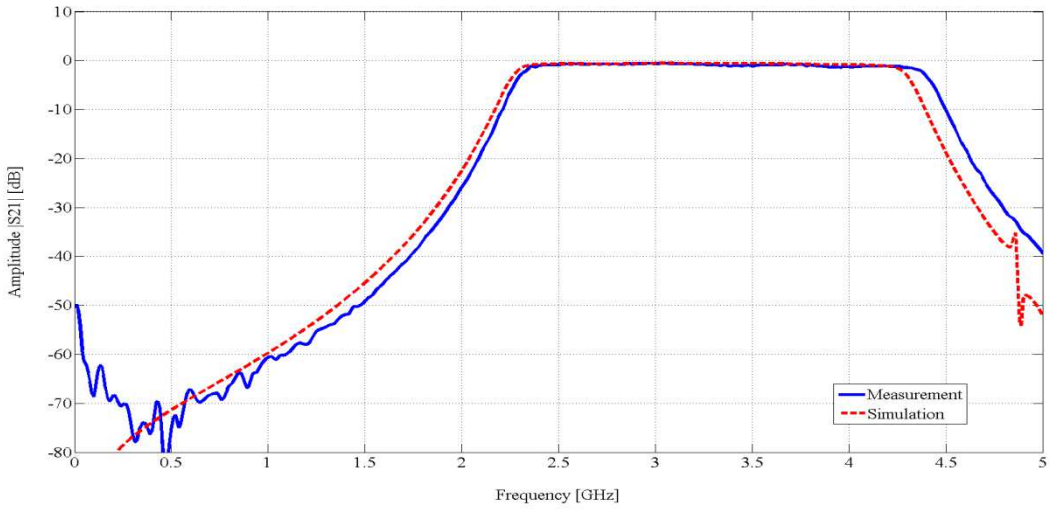

(b)

Figure 13. Simulated (dashed line) and measured (continuous line) frequency response of the short-circuited stubs band pass filter: (a) S_{11} parameters, (b) S_{21} parameters.

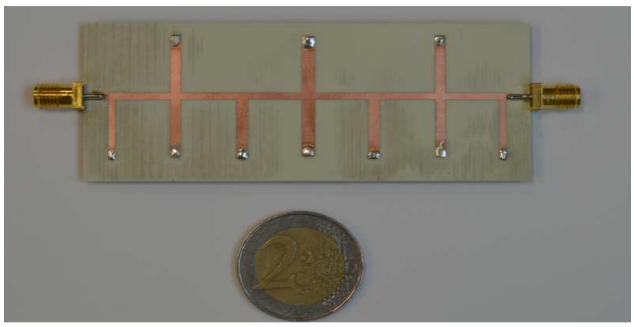

Figure 14. Layout of the fabricated 7-pole short-circuited stubs band pass filter on a Rogers RO4350E substrate with ε_r =3.66 and h=0.508 mm.

From Fig. 13, the frequency response is significantly improved compared to the previous configuration, but it is evident a frequency shift and a consequent discrepancy between the measured and simulated values. It's also clear the presence of an unwanted peak (acceptable, being less than -13 dB) on the reflection coefficient at the frequency of about 3.8 GHz, and a peak on the transmission coefficient at a frequency of about 4.9 GHz, which, however, represents a peak due to the simulation (it doesn't appear during the measurement).

As mentioned above, the welding could be considered one of the main problems during the fabrication on this type of substrate. In particular, the holes of diameter 0.6 mm (used for the creation of paths to ground), have been made at a distance of 0.3 mm from the end of the lines, while the simulation considers exactly the end of the lines; therefore, it has been considered a simulation in which the lengths of the stubs connected to the ground have been decreased by 0.3 mm, in such a way as to have an identical situation in the paths to ground.

The comparison between simulation and measurement shows an excellent agreement. The results of comparison are shown in Fig. 15. The reflection coefficient shows a clear improvement due to the frequency shift; the largest peak measured in Fig. 13 is not due to the decrease of the stubs lengths but to the welding of the connectors on the feed line.

Regarding the insertion loss, it is evident a very good agreement between the responses. The frequency shift allows to overlap the curves, maintaining the same slope, and to meet the initial specifications. Moreover, the peak present in the transmission coefficient in Fig. 13, has been deleted.

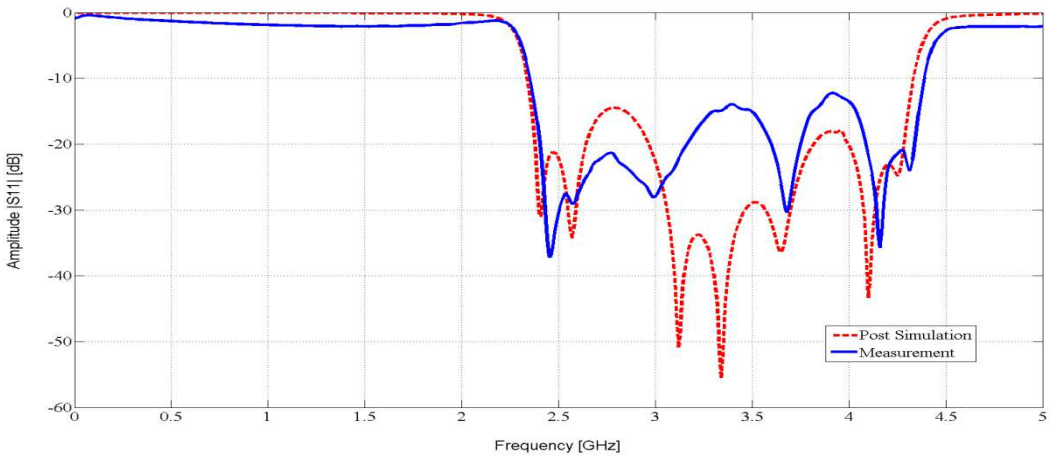

(a)

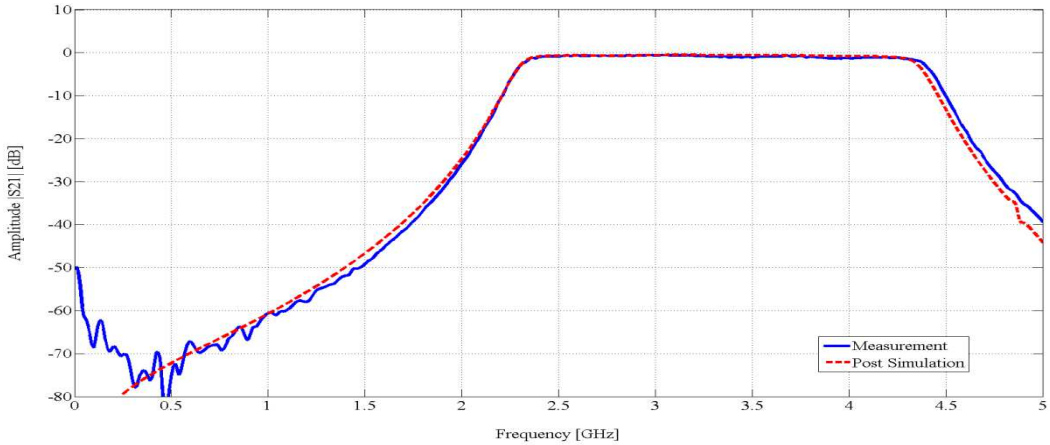

(b)

Figure 15. Simulated (dashed line) and measured (continuous line) frequency response of the short-circuited stubs band pass filter: (a) S_{11} parameters, (b) S_{21} parameters.

4.0 Conclusions

In this paper a short-circuited stubs band pass filter has been designed, simulated, optimized, fabricated and measured using the LPKF Printed Circuit Board milling machine and its parameters measured with the ROHDE&SCHWARZ ZVA 67 Vector Network Analyzer (with the ZV-Z218 calibration kit). The numerical simulation and measurement of the fabricated filter, show the validity of the analysis and of the design, mainly thanks to the study concerning the discrepancy obtained in a first phase of the comparison. The fabricated band pass filter could be used for the S-Band receiver of the Sardinia Radio Telescope. The Rogers RO4350E substrate used in this project, presents the possibility of integrating more SMD components on a single board.

5.0 Acknowledgments

We gratefully acknowledge A. Ladu for the help during the realization of the circuitries.

6.0 References

[1] G. Y. Zhang, F. Huang, and M. J. Lancaster, “Superconducting spiral filters with quasi elliptic characteristic for radio astronomy,” *IEEE Trans. Microw. Theory Technol.*, vol. 53, no. 3, pp. 947–951, Mar. 2005.
[2] http://www.rogerscorp.com/documents/726/acm/RO4000-Laminates---Data-sheet.pdf
[3] G. Valente G. Serra, F. Gaudiomonte, A. Ladu, T. Pisanu, P. Marongiu, A. Corongiu, A. Melis, M. Buttu, D. Perrodin, G. Montisci, G. Mazzarella, E. Ergon, N. Iacolina, C. Tiburzi, V. Vacca, “A MultiFeed S-Band Cryogenic Receiver for the Sardinia Radio Telescope Primary Focus”.
[4] JiaShen G.Hong, M.J.Lancaster, “Microstrip Filters for RF/Microwave Applications”, John Wiley &Sons Inc., 2001.
[5] Radiall - Innovator of Interconnect Components & More - www.radiall.com.